Frozen mode from hybridized extraordinary transmission and Fabry-Perot resonances

M. Beruete,* P. Rodriguez-Ulibarri,† and V. Pacheco-Peña‡
TERALAB (MmW—THz—IR & Plasmonics Laboratory), Universidad Pública de Navarra, Campus Arrosadía, 31006 Pamplona, Spain

M. Navarro-Cía§
Optical and Semiconductor Devices Group, Department of Electrical and Electronic Engineering, Imperial College London, London SW7 2BT, UK,
Centre for Plasmonics and Metamaterials, Imperial College London, London SW7 2AZ, UK, and
Centre for Terahertz Science and Engineering, Imperial College London, London SW7 2AZ, UK

A. E. Serebryannikov‖
Hamburg University of Technology, E-3, D-21071 Hamburg, Germany
(Received 23 March 2013; published 21 May 2013)

Frozen modes arising in stacked subwavelength hole arrays are studied in detail. Their origin is proved to be connected with the interaction between the extraordinary transmission resonance and the Fabry–Perot cavity mode. The analysis is done for various situations that differ in metal plate thicknesses and sizes and shape of the holes. Dispersion results and finite-stack transmission spectra are in good agreement, both showing the features indicating hybridization. The boundaries of the hybridization are found in terms of the geometrical parameters. The effect of the number of stacked plates on the transmission has been demonstrated. Finally, it is shown that the group index of refraction n_g in the considered finite structures can be larger than 200. The obtained estimates of n_g, which are based on dispersion and transmission results, well coincide with each other.

DOI: 10.1103/PhysRevB.87.205128 PACS number(s): 42.25.Fx, 42.79.Dj, 41.20.Jb, 78.67.Pt

I. INTRODUCTION

Periodic structures have historically played a prominent role in electromagnetism, mainly to offer control of the electromagnetic radiation. In general, their properties arise from the particular arrangement and geometry of the constituent particles, i.e. unit cell, rather than from their specific nature or chemical composition. Hence, they have been successfully employed for synthesizing artificial media, usually with features not directly available or difficult to find in natural materials. Following this concept, artificial dielectrics, i.e. metallodielectric structures engineered to obtain an effective electric response, were the subject of intensive investigation decades ago.[1] Also, the roots of artificial magnetism can be found in the book of Schelkunoff.[2] In the late 1980s, photonic bandgap structures were proposed to control radiation and propagation of light.[3,4] More recently, artificial magnetism has been exploited[5] and has given rise to the topic of metamaterials.[6,7] At difference with artificial dielectrics, metamaterials offer the possibility to control at will not only the electric response but also the magnetic response, widening the applicability of artificial materials substantially.

Periodicity is also essential in the topic of plasmonics, a discipline devoted to the control of light using surface waves at metal-air/dielectric interfaces. In fact, extraordinary transmission (ET) structures, which were central for the development of this topic, rely fundamentally on periodicity.[8,9] A tight link between metamaterials and ET was found in the past by using a periodic stack of ET hole arrays.[10,11] Again, periodicity was crucial for the performance. If the stack period was short in terms of operation wavelength, a backward-wave appeared inside the structure, also called left-handed (LH) propagation. In turn, if the period was relatively large, the wave inside the structure was of the forward type, also called right-handed (RH) propagation. In between, the mode inside was ideally neither backward nor forward, and rather a "frozen-mode" appeared[11] (although, in a realistic case, this mode has a small but nonzero slope and, strictly speaking, is either forward or backward despite being very slow).

The band structure of stacked hole arrays depends mainly on two factors:[11,12] stack period (d_z) and in-lattice period (d), which govern, respectively, the fundamental Fabry–Perot (FP) mode of the cavity enclosed by consecutive hole arrays, and the onset of the (0,−1) diffraction mode (following the notation of Ref. 13) or Rayleigh–Wood's anomaly[14] that gives rise to the ET resonance. The third factor that can produce a band is an aperture resonance, which happens at the cutoff frequency of the fundamental mode supported by the hole.[12] This last case has received a lot of attention in the context of ET, and theoretical models have been proposed to explain the enhancement of transmission near the aperture resonance.[15] Even more, related with the content of this paper, slow-group velocity modes associated with this resonance have been detected,[16] and the interaction between FP modes and aperture resonances (dubbed localized surface plasmon resonances) has been analyzed.[17] It is worth mentioning that a resonant slot was easily explained by Booker in his seminal paper of 1946[18] by observing that a rectangular aperture on a metallic screen is the complement of a half-wave dipole, in terms of Babinet's principle, and since then has been commonplace for microwaves and antenna engineers. In fact, the well-known, pervasive, and cost-effective slot antennas operate following this rationale. Moreover, it is arguable to label this resonance as ET, since the aperture is not strictly subwavelength (by definition, it is operating very near cutoff). For these reasons, we will leave aside the aperture resonance regime and concentrate only on ET and FP resonances. In

Ref. 11, RH, LH, and frozen-mode propagation were described and experimentally demonstrated in stacked subwavelength hole arrays. Right-handed propagation for large periods was explained as a FP type passband. In Ref. 12, a modal analysis led to similar conclusions. In Refs. 19 and 20, FP modes inside a stacked mesh-grid structure with a rather weak metallization were studied in depth. Several papers can be found in the literature analyzing LH propagation. In Refs. 10 and 11, it was explained in terms of an inverse transmission line model. The modal analysis performed in Ref. 12 also led to a similar inverse transmission line model. A pure equivalent circuit explanation for a stack of only two plates—usually called as fishnet structure—can be found in Ref. 21.

Frozen-modes or slow-light regimes have been intensively investigated since the seminal experiment by Hau *et al.* demonstrating electromagnetically induced transparency (EIT) and light velocity reduction up to 17 m/s.[22] Slow light has a strong technological significance, allowing applications such as all-optical processing and optical storage, see Refs. 23–26 and references therein. Metamaterials have already been employed in slow-light regimes proposing fascinating applications such as a trapped rainbow.[24] Photonic crystals are also typically used for slow-wave applications,[26,27] as well as magnetic photonic crystals.[28,29]

In this paper, we study numerically details of appearance and main features of frozen modes in stacked ET hole arrays with the emphasis put on clarifying their nature. This regime has been studied experimentally in the past[11] in stacked hole arrays where it has been proposed for absorbers.[30] However, a thorough analysis to unveil the ultimate mechanism of the slow-light regime was not given yet. First, a dispersion based study is carried out in order to observe the evolution of the bands as a function of the stack period for several hole sizes and shapes and metal thicknesses. It will be shown that the origin of the frozen mode is related to the interaction between ET and FP resonance and can be controlled by variations in hole size, stack period, and metal thickness. This will be confirmed by a finite stack analysis, where the fields of the different transmission peaks will be examined. In particular, multiple total-transmission peaks can be obtained in the lossless case for various numbers of stacked plates, whose spectral positions are in good coincidence with the predictions that are based on the dispersion results. The metallic plates are assumed to be perfect electrical conductors, so that the obtained results are scalable, provided that the losses remain relatively low. The results presented in this paper are obtained using CST Microwave Studio.[31] Throughout this paper, normalization with respect to the hole period d is used for all the magnitudes except for the propagation constant along z which is normalized with respect to the stack period $\beta = \beta' d_z$. Therefore, a normalized frequency will be used, $f = f'd/c$, where f' is the physical frequency, and c is the speed of light in vacuum.

II. DISPERSION ANALYSIS OF INFINITE STRUCTURES

A. Small holes and infinitesimally thin plates

The first structure analyzed is a square metallic hole array with periodicity d and infinitesimal thickness perforated with square holes of side $a = d/6$, see schematic in Fig. 1(a). The dispersion diagrams for the two lowest passbands of the structure—assumed infinite along all three axes—and several stack periods ranging from $d_z = 0.38d$ to $0.6d$ were obtained using the eigenmode solver of CST Microwave Studio. In order to achieve accurate results and discretize accurately the sample, a denser local mesh has been applied to the aperture. The minimum edge length in the simulation is $16 \times 10^{-3}\, d$, whereas the maximum edge length is $16 \times 10^{-2}\, d$. The propagation direction was assumed here to coincide with the stacking direction z, and a vertical polarization was used E_y.

As mentioned in the introduction, the band structure depends mainly on two factors: the stack period (d_z) and in-lattice period (d), which govern the FP and the ET resonance, respectively. These resonances happen when

$$f = f_{\mathrm{FP}} \approx d/2d_z, \tag{1a}$$

$$f = f_{\mathrm{ET}} \approx 1. \tag{1b}$$

The third factor that can produce a band is a slot resonance. However, due to the small hole size, this resonance will be out of the frequency span considered ($f_{\mathrm{cutoff}} = 3$) and will be neglected in the subsequent analysis.

Figure 1 presents dispersion results as well as the electric field distribution when the first two bands do not interact. Looking at the dispersion results of Figs. 1(d) and 1(e), it is found that, in general, the FP band extends from the FP resonance condition (represented as dashed grey lines in the figure) downwards. If the stack period is small enough so that the FP band lowest edge is above $f = 1$, then there is no band interaction and the first and second bands correspond entirely to ET or FP resonances, governed by d and d_z, respectively, see Fig. 1(d). Similarly, when the stack period is so large that the FP cavity resonance falls entirely below the lowest ET band edge, separation between the bands occur again, so the first band corresponds entirely to the FP resonance and the second band does to the ET resonance, see Fig. 1(e).

From the comparison of these two cases, it can be concluded that, if geometrical parameters are chosen so that ET and FP resonances are sufficiently far away, the nature of each band does not depend on variation of the stack periodicity but only on the type of resonance. In short, the ET band is totally determined by the hole array periodicity d (upper limit around f_{ET}), is always LH, and its bandwidth is larger for small stack periods.[10–12] On the other hand, the FP band is totally determined by the stack period d_z (upper limit around f_{FP}), is always RH, and has a narrow bandwidth as well. Attending to the modal field pattern, within the ET band, the electric field is contained mainly along the longitudinal direction, so that E_z dominates over E_y [Fig. 1(b)] contrarily to what happens at the FP resonance where E_y is noticeably stronger than E_z [Fig. 1(c)]. We will use these features in the subsequent discussion to identify the ET or FP nature of the resonances. Also, note that these plots have been obtained for a phase difference between input and output (periodic) ports $\beta d_z = 0^\circ$.

Things are completely different when $f_{\mathrm{FP}} \approx f_{\mathrm{ET}}$. This condition implies that $d_z \approx d/2$. In turn, it corresponds to the case when a frozen mode appears.[11] To analyze in detail this case, the dispersion diagram has been obtained for stack periods near this condition. The results are presented in Fig. 2(a). At $d_z \approx 0.492d$, the resonances are still fully

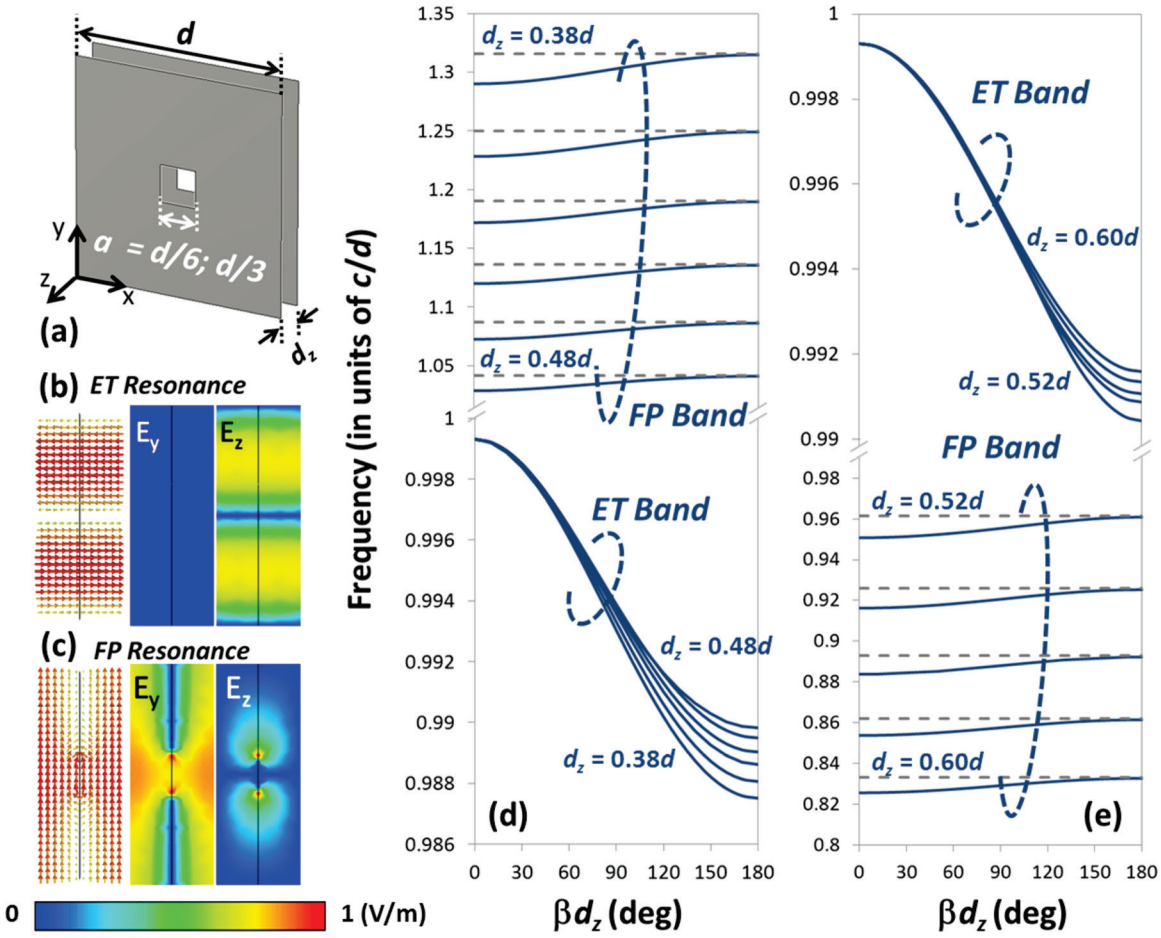

FIG. 1. (Color online) (a) Schematic of the unit cell of a square hole array of infinitesimal thickness and square aperture, along with the relevant dimensions. Cross-sectional view of the electric field at (b) ET resonance and (c) FP resonance. Calculated dispersion diagram of a hole array with $a = d/6$ and infinitesimal thickness when the first two bands and decoupled so that the FP band is either entirely (d) above the ET band or (e) below the ET band. Grey dashed lines correspond to the analytical fundamental FP resonance frequency calculated with Eq. (1a).

separated, and the behavior of the dispersion curves is similar to that in Fig. 1(d). However, a slight increment of the stack period $d_z = 0.496d$ makes the FP band tail meet the ET band top edge, setting off band interaction. From this point on, it is no longer possible to establish an unambiguous correspondence between the bands and types of resonances, i.e. ET or FP. So, this notation will be left aside, and we will refer subsequently to each band simply as first (low frequency) or second (high frequency) bands.

Looking closely at the cases $d_z/d \in [0.496, 0.498]$, we can establish a qualitative analysis. First, it is observed that the second band top edge is always near f_{FP}, suggesting a FP resonance, as usual. As for the second band bottom edge, it would normally fall below $f = 1$, following the tendency of smaller stack periods. However, the Rayleigh–Wood's anomaly imposes a strict bandstop condition precisely at $f = 1$. This singularity is governed by in-lattice period d and cannot be overridden by the cavity mode, resulting in a band edge exactly at $f_{\mathrm{ET}} = 1$. This suggests that this point has an ET resonance nature. However, below the extreme singularity of the Rayleigh–Wood's anomaly, the FP resonance still has some energy stored and pushes the first band top edge downwards. More technically, this can be interpreted as a direct consequence of Foster's theorem, which forces alternating poles and zeros in the frequency response of passive structures such as frequency selective surfaces.[32] In physical terms, this behavior is usually called band hybridization[33] that results from the interaction of two different resonances. Since the shift of the first band top edge is an outcome caused by d_z, it can be attributed to a cavity effect, i.e. a FP resonance. The first band bottom edge remains at the same location as in all previous cases, so it should correspond to an ET resonance. From this picture, it is then clear that, in this stack period interval, the resonance nature at the band edges flips in both bands from ET to FP and vice versa. Consequently, out of the band edges, the modes must be strongly hybridized so that the fields show the features typical for both ET and FP resonances. This hypothesis is demonstrated subsequently while discussing the case $d_z/d = 0.5$, which is highly remarkable since the bands become almost perfectly flat. As for the handedness, it is noticed that, despite the hybridization, the first band remains LH and the second band RH in this interval.

At the critical distance of $d_z/d = 0.5$, both the FP condition and the Rayleigh–Wood's anomaly exactly correspond to

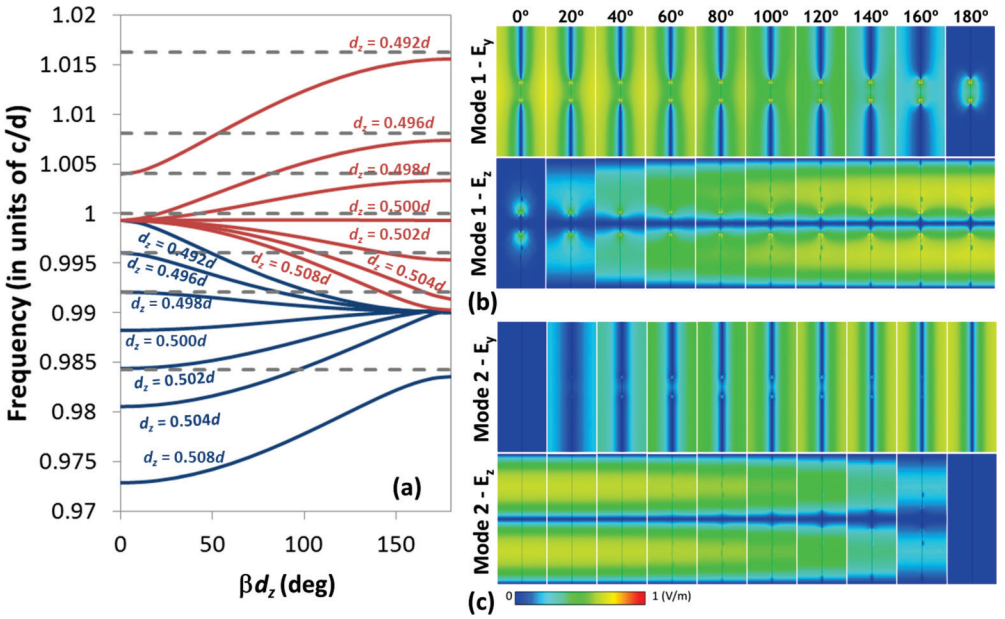

FIG. 2. (Color online) (a) Band diagram of the hole array of Fig. 1(a) around the frozen-mode condition $d_z \approx d/2$: as explained in the text, due to band interaction, it is no longer possible to establish an explicit correlation between bands and resonances (ET or FP), so bands are labeled as first band (blue) and second band (red). Complete sequence of the electric field pattern evolution at $d_z = d/2$ as βd_z varies from 0° to 180° with a step of 20°: (b) first mode and (c) second mode (E_y above and E_z below in each panel). Grey dashed lines correspond to the analytical fundamental FP resonance frequency calculated with Eq. (1a).

the same frequency $f = 1$. In this situation, there are two resonances, which are indeed very different in nature (ET governed by d and FP governed by d_z), competing to share exactly the same spectral location. This provokes such a strong modal interaction that both bands become nearly flat (the first band has a tiny positive slope, so it is "flatter" at a slightly smaller distance) and, moreover, emerge very near in frequency, one at $f = 0.99$ and another at $f = 1$. At this point, band hybridization is taken to the extreme. Looking at the electric field in each band, it is observed that the field distribution changes gradually as the phase is varied, see Figs. 2(b) and 2(c) where a complete sequence of the electric field pattern evolution is shown for both bands, varying the phase from 0 to 180° with a phase step of 20°. In particular, the first band switches from FP at $\beta d_z = 0^\circ$ to ET at $\beta d_z = 180^\circ$ even though the frequency remains almost unchanged. The percentage bandwidth is here just 0.19%. The second band does exactly the opposite switching from ET to FP, within a negligible percentage bandwidth of just $5.7 \times 10^{-5}\%$. Putting it in a slightly different way, the frequency remains almost constant as the phase is varied, but the field distribution is completely different (and is swapped in bands) at the band edges. In the middle, the modes are neither ET nor FP, but rather a hybrid between these resonances.

This behavior is maintained as long as band interaction is present. It is interesting to observe that, for stack periods $d_z/d \in [0.502, 0.504]$, the first band becomes RH and the second band LH, but it has been observed that the modal swapping between edges is exactly as before (not shown here). Finally, when $d_z/d = 0.504$, both bands begin to detach from each other until they are again completely separated at $d_z/d = 0.508$. At this point, the first band is totally due to the FP resonance, and the second is caused by a conventional ET resonance, without any band hybridization. A summary of the behavior of both bands at the edges is presented in Table I.

So, the physical mechanism underlying the frozen-mode regime is clearly the interaction between ET and FP resonance. When both compete to share the same spectral location, hybridization occurs, and then two narrow frozen-mode bands appear. Interestingly, none of them can be unambiguously related either to ET or to FP resonances. Rather, the field pattern demonstrates that each band behaves purely either as ET or FP at the extremes $\beta d_z = 0^\circ$ and $\beta d_z = 180^\circ$ and are strongly hybridized in the middle.

B. Medium-sized holes and infinitesimally thin plates

Increasing the hole size to $a = d/3$ (now $f_{\text{cutoff}} = 1.5$ so we are still within the ET limits, $f_{\text{ET}} < f_{\text{cutoff}}$), widens the ET bandwidth, see Fig. 3(a), a feature that was already observed in Refs. 9 and 12. The FP bandwidth is also increased since now the metal in the plates is reduced, and their reflectivity must diminish accordingly. So, the cavity resonance condition is less strict, and the FP resonance is less sharp than for small

TABLE I. Dominant resonance at the band edges as a function of the stack period. Hole arrays of infinitesimal thickness and $a = d/6$.

Normalized stack	First band		Second band	
period	$\beta d_z = 0^\circ$	$\beta d_z = 180^\circ$	$\beta d_z = 0^\circ$	$\beta d_z = 180^\circ$
$d_z/d \leqslant 0.496$	ET	ET	FP	FP
$0.496 < d_z/d \leqslant 0.504$	FP	ET	ET	FP
$d_z/d > 0.504$	FP	FP	ET	ET

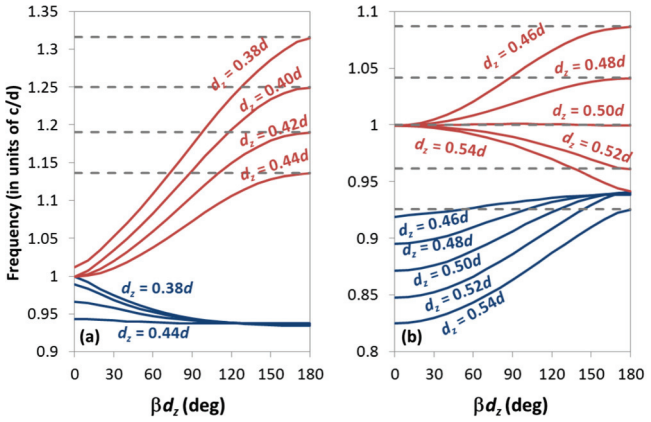

FIG. 3. (Color online) Calculated dispersion for a hole array with $a = d/3$ and d_z varied from $0.38d$ to $0.54d$. For the sake of clarity, the figure is divided in two panels (a) and (b). Grey dashed lines correspond to the analytical fundamental FP resonance frequency calculated with Eq. (1a).

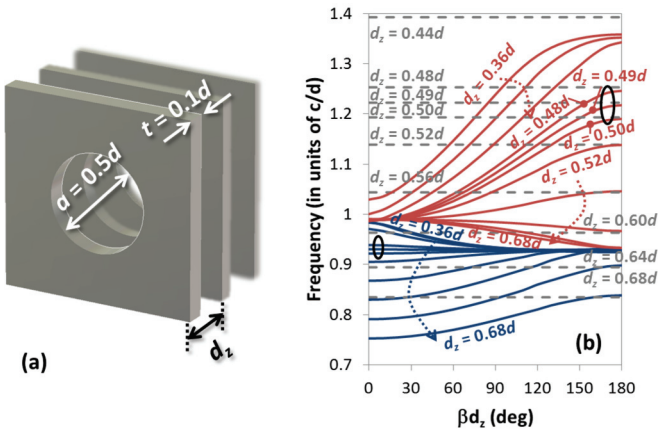

FIG. 4. (Color online) (a) Schematic of unit cell of the stacked hole arrays with finite thickness and circular holes along with relevant dimensions. (b) Dispersion for such structures for d_z from $0.36d$ to $0.68d$ in step of $0.04d$, with a finer step near the frozen-mode condition $d_z = 0.48d$, $0.49d$, and $0.50d$, highlighted with a black ellipse in the curve. Grey dashed lines correspond to the analytical fundamental FP resonance frequency calculated with Eq. (1a) and the cavity length conveniently modified, as explained in the text. Black ellipses delimit the region where the first band becomes almost flat.

holes, i.e. the quality factor is reduced, and the bandwidth is enlarged. This implies that the FP band bottom tail encounters the ET band top edge for a stack period as small as $d_z/d = 0.4$, pushing the ET band downwards. This is the limit where band interaction and hybridization start. A summary of the bands' edges' performance obtained from the observed field distribution at each point is shown in Table II for different values of the stack period.

An important consequence of the increment of the hole size is that, now, the first and second bands become flat at different stack periods: at $d_z/d = 0.44$ and $d_z/d = 0.5$, respectively, compare Figs. 3(a) and 3(b). This means that it is possible to excite two different frozen modes at different frequencies for two different stack periods.

C. Stacks of finite-thickness arrays with circular holes

In practice, hole arrays have nonnegligible thickness. Also, for fabrication purposes, it is sometimes easier to drill circular holes, rather than square ones. Thus, here, we concentrate on realistic hole arrays similar to those employed in Refs. 9–11 with finite thickness $t = 0.1d$ and circular apertures of diameter $a = 0.5d$, see schematic in Fig. 4(a). Now, the cutoff frequency is $f_{\text{cutoff}} = 1.2$.

Strictly speaking, now, the cavity length is $d_z - t$, so the FP resonance should happen at $f_{\text{FP}} \approx 0.5d/(d_z - t)$. However, since the field penetrates through the apertures, the effective cavity length is somewhat larger. A good fitting is obtained when the cavity length is approximated as $d_z - 0.081d$, putting the FP resonance at $f_{\text{FP}} \approx 0.5d/(d_z - 0.081d)$. Looking at the dispersion results of Fig. 4(b), it is observed that, for small stack periods $d_z/d \in [0.36, 0.44]$, the top edge of the second band is noticeably below the FP resonance condition. What happens here is that, following the notation of Ref. 34, near the onset of the $(\pm 1, -1)$ diffraction mode at the normalized frequency $f = \sqrt{2}$, there is another band (not shown) which interacts with the second one and pushes it downwards. However, study of this effect is beyond the scope of this paper. Concentrating on the first and second bands, it is seen that interaction starts at $d_z = 0.44d$. At $d_z = 0.48d$, the FP cavity condition effectively determines the top edge of the second band, and moreover, interaction between first and second band is more accentuated. In the interval $d_z/d \in [0.48, 0.50]$, the first band becomes nearly flat. The frequency excursion at $d_z = 0.49d$ is less than 0.07%. As in the previous case, the second band is nearly flat at a different periodicity $d_z = 0.58d$, with a frequency variation of 1.5%. Interaction lasts until a sufficiently large period is reached $d_z = 0.64d$. Finally, a summary of the bands' edges' performance obtained from the observed field distribution at each point is shown in Table III for different values of the stack period.

TABLE II. Dominant resonance at the band edges as a function of the stack period. Hole arrays of infinitesimal thickness and $a = d/3$.

Normalized stack	First band		Second band	
period	$\beta d_z = 0°$	$\beta d_z = 180°$	$\beta d_z = 0°$	$\beta d_z = 180°$
$d_z/d < 0.4$	ET	ET	FP	FP
$0.4 \leqslant d_z/d \leqslant 0.52$	FP	ET	ET	FP
$d_z/d > 0.52$	FP	FP	ET	ET

TABLE III. Dominant resonance at the band edges as a function of the stack period. Hole arrays of $t = 0.1d$ and circular apertures of diameter $a = d/2$.

Normalized stack	First band		Second band	
period	$\beta d_z = 0°$	$\beta d_z = 180°$	$\beta d_z = 0°$	$\beta d_z = 180°$
$d_z/d \leqslant 0.44$	ET	ET	FP	$(\pm 1, -1)$
$0.44 < d_z/d \leqslant 0.64$	FP	ET	ET	FP
$d_z/d > 0.64$	FP	FP	ET	ET

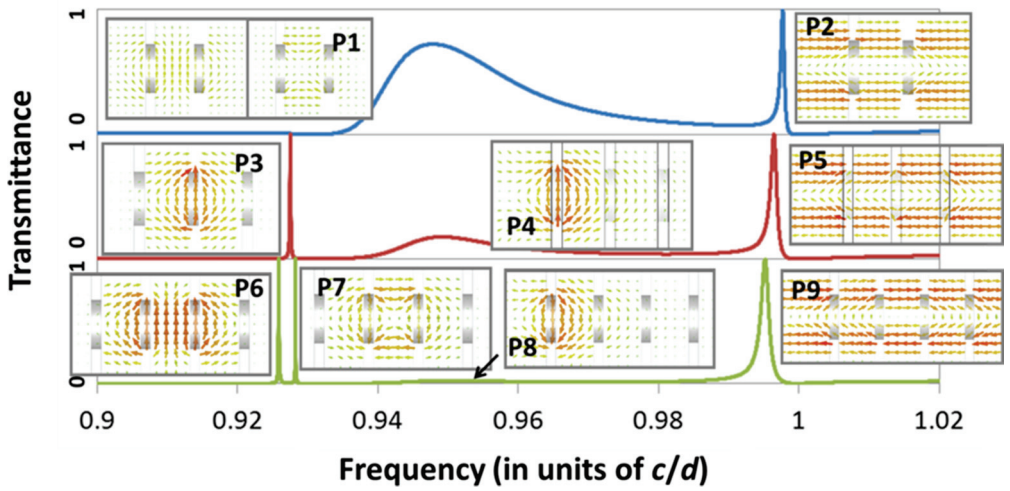

FIG. 5. (Color online) Transmittance of realistic hole arrays with finite thickness $t = 0.1d$ and circular apertures of diameter $a = 0.5d$ at the frozen-mode operation $d_z = 0.5d$ for $N = 2$ (blue), 3 (red), and 4 (green) plates. (Insets) Electric field at the peaks observed in the spectra.

III. FINITE STACKS: TRANSMISSION SPECTRA AND MODAL DISTRIBUTIONS

Next, the transmission spectra of structures with a finite number of stacked plates were analyzed. The study was particularized to the structure discussed in Sec. II C, which is the most interesting from a practical point of view. Normal incidence $\theta = 0^\circ$ and the critical distance $d_z = 0.5d$ were considered, while the number of stacked plates N was varied. In Fig. 5, the spectra corresponding to $N = 2$ (blue), 3 (red), and 4 (green) are shown along with the field distribution at notable points.

The first peak for $N = 2$ (P1) appears at $f = 0.95$ and has a transmittance of 0.7. Two snapshots at different time slots are shown in the inset. As seen, the field oscillates and twists inside the structure with the result that y component (leftmost inset of top plot) dominates at one time slot, whereas the z component (central inset of top plot) dominates at the other. Also, the magnitude of both components E_y and E_z is similar so it has traces of both FP and ET resonances. This peak shifts towards higher frequencies and decays abruptly as N is increased (P4, P8). This is a clear fingerprint of the interaction between FP and ET resonances: when they are well separated from each other, the ET band appears at this frequency range, as shown in the dispersion diagram of Fig. 4(b) and in the transmittance plots of Fig. 5. However, when band interaction occurs, a bandgap appears around $f = 0.95$. So, the mode in this case is evanescent, power decays exponentially through the structure, and transmittance is noticeable only for a small number of stacked plates.

A new total-transmission peak (P3) appears around $f = 0.925$ when taking $N = 3$ instead of $N = 2$. This peak corresponds to the frozen-mode shown in the dispersion results of Fig. 4(b) and discussed deeply in Ref. 11. It is remarkable that this band only appears for stacks of more than two plates, in good agreement with the experimental results of Ref. 11. As explained in Ref. 11, the frozen-mode has a dynamic nature in the sense that it only appears for periodic structures, and obviously, the minimum structure to be considered periodic is a three-plates stack. Here, we have found that the frozen mode arises due to the interaction of FP and ET resonances. Moreover, the electric field plot shows that the field is confined around the central plate, and its distribution is very similar to that at P4 and P8, see the left panel in the middle plot. However, in contrast to P4 and P8, it is localized for P3 around the central plate, a situation that is not possible for only two stacked plates. This clearly confirms that FP and ET resonances are fully interacting: the resonance is confined inside the stack, and moreover, the resonance frequency happens exactly at the otherwise tail of the ET band. At $N = 4$, two peaks appear (P6 and P7), whose field pattern presents even and odd symmetry with respect to the central x-y plane, respectively. Also, between the second and the third plates, E_y dominates over E_z at P6, implying a mostly FP-like mode, whereas the contrary is true for P7, implying a mostly ET-like mode. This is in perfect agreement with our analysis in terms of dispersion diagrams, see Sec. II and especially Table III. Also, all these peaks can be identified as internal modes.[34]

The total-transmission peak around $f = 1$ (P2, P5, and P9) is located near the lower edge of the second band. This corresponds to the well-known external mode or long-range spoof plasmon,[9–13,34–36] which always appears near the Rayleigh–Wood's anomaly, and has an obvious ET nature, as predicted by our previous analysis; as shown in Fig. 5, E_z dominates clearly over E_y, and the field pattern presents odd symmetry with respect to the central x-y plane.

Figure 6 gives a wider view of the transmittance under normal incidence when the number of the stacked plates N and stack period d_z are varied from two to four and from $0.36d$ to $0.7d$, respectively. The structure thickness in each case is $D = t + d_z(N - 1)$. In Fig. 6, the horizontal axis represents the normalized frequency, the vertical axis represents the normalized stack period, and the color scale the transmittance in dB. The figure is plotted for the region of interest where the frozen mode arises, i.e. around $d_z = 0.5d$ and $f = 1$. The insets show a wider view. Superimposed in the insets (cyan line) is

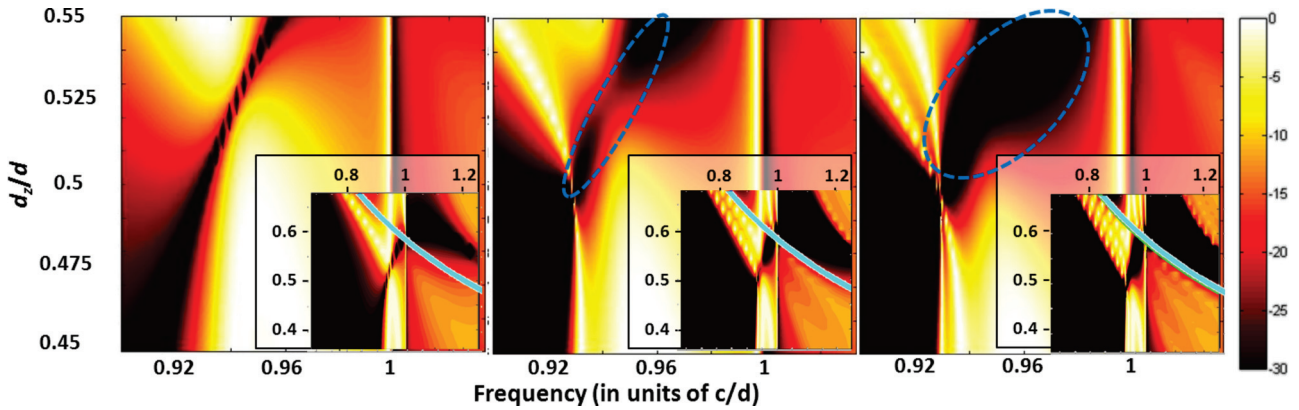

FIG. 6. (Color online) Contour maps of the transmittance in dB scale for realistic hole arrays with finite-thickness plates $t = 0.1d$ and circular apertures of diameter $a = 0.5d$ as a function of frequency and stack period at $N = 2$ (left), 3 (middle), and 4 (right). Insets: wider view with the full calculation spectra and a wider range of d_z. Superimposed in the insets (cyan line) is the calculated FP resonance frequency.

the FP resonance frequency calculated as $f_{FP} \approx 0.5d/(d_z - 0.081d)$.

From Fig. 6, it is obvious that the minimum of transmission is introduced by the Rayleigh–Wood's anomaly at $f = 1$ for all stack periods and number of plates. Also, the transmittance is always larger when the band is located below $f = 1$, regardless of the nature of the band. This can be explained invoking equivalent circuit arguments: the admittance of the first high-order mode responsible for ET (TM_{02} in the artificial waveguide of mutually orthogonal electric and magnetic walls) is purely imaginary below Wood's anomaly, whereas it is purely real above Wood's anomaly, leading to an inevitable impedance mismatch. This will be analyzed in detail in a subsequent paper. For small stack periods $d_z/d < 0.45$, ET and FP bands are clearly separated in the spectra, being the first noticeably more intense. Around the condition $d_z/d = 0.5$, ET and FP bands merge. Again, no trace of a frozen mode is detected for two plates, whereas for three and four plates a very narrow peak in the vicinity of $f = 0.93$ and another around $f = 1$ appear. The frozen mode becomes better pronounced as the number of plates increases. Due to the band interaction, there arises a region of very low transmission approximately between $0.5 < d_z/d < 0.55$ and $0.93 < f < 0.99$, which is highlighted in Fig. 6 by dashed blue line ellipses. Again, the higher number of plates, the more emphasized this mechanism is. Finally, for larger periods, the FP band is located below the ET band. Note that in this case the number of peaks in the FP band is always $N - 1$, in good agreement with a FP cavity mode nature. Note that this behavior is also in very good agreement with the dispersion diagram of Fig. 4(b).

IV. GROUP INDEX: FINITE STACK AND DISPERSION DIAGRAM

The appearance of slow electromagnetic waves in transmission is a fingerprint of frozen modes. To characterize transmission in the infinite stacked hole-array structure, the standard formula for the group velocity (v_g)

$$v_g = d\omega/d\beta \tag{2}$$

can be used. The corresponding values of the group refractive index can be found as follows:[37]

$$n_g = c/v_g = n_p + \omega dn_p/d\omega, \tag{3}$$

where n_p is the phase refractive index defined as $n_p = \omega/\beta$.

Figure 7 presents the frequency dependence of n_g at $d_z = 0.5d$, which is inferred from the dispersion results, i.e. by using Eq. (3). Also, the group index is estimated from the transmission results obtained for N varied from 2 to 10. The latter has been obtained by using the standard procedure based on the formula:[26]

$$n_g = c/2D\,(f_2 - f_1)\,, \tag{4}$$

where D is the total thickness, f_1 and f_2 are the frequencies of two adjacent peaks. The obtained value of n_g is usually assigned to the mid frequency. In the inset of Fig. 7, the transmission spectra are shown for the frozen-mode band. Most of them represent a sequence of transmission peaks whose number depends on N. One can see that it is always equal to $N - 2$, as follows from our discussion in Sec. III. For this reason, the group index in the finite stack structure is calculated only for four plates onwards. It is worth noting that the peaks at the right edge of the band are also expected

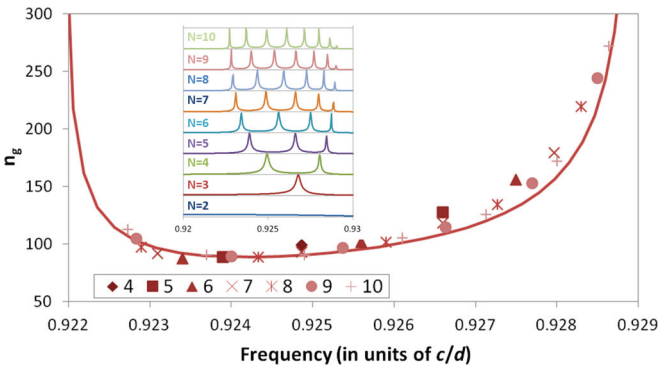

FIG. 7. (Color online) Group index of refraction obtained from transmission results (symbols) and from the dispersion diagram (solid line) at various N. Inset: transmission spectra for N varied from 2 to 10.

to correspond to the total transmission, as might be obtained from more accurate simulations.

The coincidence of the results obtained by both methods is quite good. A minimum value of $n_g = 87.62$ is obtained, according to the dispersion results, somewhere in the center of the first half of the frozen-mode passband. Both dispersion and transmission-based estimates show that $n_g > 200$ can be obtained in the finite structures at $N > 7$. Clearly, the larger N, the larger n_g can be obtained at the peak being nearest to the band edge. To compare, $n_g = 14$ and $n_g > 60$ have been reported at optical frequencies for the coupled resonator structures[25] and photonic crystal slabs working in the defect-mode waveguide regime,[26] respectively. In addition, $n_g = 220$ for a photonic crystal working in the defect-mode transmission regime at microwave frequencies has been demonstrated.[38] Ultrahigh values of n_g, e.g. $n_g = 2 \times 10^9$ are known to be obtainable in the EIT slow-light optical buffers.[25] As a final word on this subject, it is worth mentioning that we have particularized the analysis to the case $d_z = 0.5d$, since this is the one that we had characterized in Ref. 11. We have found numerically a maximum value of $n_g = 1442$ for $d_z = 0.49d$. However, the strong dispersion of the structure as well as the difficulty to experimentally ensure that all plates are placed at exactly the same distance prevents us from putting the focus on this ideal high value. Our main goal here was to elucidate the origin of the frozen mode in stacked hole arrays, rather than claiming an astonishingly low value of group velocity.

V. CONCLUSIONS

In this paper, a comprehensive analysis of the nature of frozen-mode regimes in stacked ET hole arrays has been presented. By performing a dispersion study, it has been demonstrated that frozen modes appear due to the interaction between FP and ET resonances. When both are sufficiently far apart, interaction disappears, and then FP band is entirely related to the stack period and ET band to the in-lattice period. However, near the frozen-mode condition, the ET and FP type modes can be strongly hybridized, sharing features of each other within a single band. Moreover, at the band edges, the modal distribution is swapped from ET to FP and vice versa. For the studied hole array geometries, it has been observed that, as the aperture size increases, band interaction starts for smaller stack periods, permitting the existence of two different frozen bands at different stack periodicities. Besides, modal properties have been analyzed for stacks of realistic hole arrays, showing nonnegligible thickness, so that the difference compared to the infinitesimal thickness case is in the field penetration through the holes that tunes the FP cavity condition.

Transmission analysis has also been done for the finite stacks of hole arrays that are composed of the plates with certain thickness. A very good agreement with the dispersion results for the corresponding infinite stack has been obtained by comparing the band location in the dispersion diagram with the peak appearance in the transmittance of finite stacks. Also, the field distribution at each peak appearing in the spectra has been analyzed, demonstrating unequivocally the strong hybridization at the frozen-mode regime. Finally, the behavior of the group index of refraction has been studied, based on both dispersion and transmission results, with an overall good agreement. A group index around 90 at the central frequency and more than 200 at the band edges has been found for the finite stacks. It must be pointed out that all the analysis is done for lossless structures. In the presence of losses, the quality factor of the frozen-mode band is expected to diminish, or equivalently, the band must widen. With this qualitative interpretation, it is clear then that the slope of the frozen-mode band would deviate from zero, giving as a result a reduction in the group index magnitude. These results could be interesting for applications such as field concentrators used to enhance field interaction with matter, sensors, filters, absorbers, frequency selective surfaces, spatial filters, etc.

ACKNOWLEDGMENTS

This work was supported in part by the Spanish Government under Contract Consolider Engineering Metamaterials CSD2008-00066 and Contract TEC2011-28664-C02-01. M.B. is sponsored by the Spanish Government via RYC-2011-08221. P.R.U. is sponsored by the Government of Navarre via program "Formación de Tecnólogos" 055/01/11. M.N.C. is supported by the Imperial College Junior Research Fellowship. A.E.S. thanks Deutsche Forschungsgemeinschaft for partial support of this work under Project No. SE1409/2-2. In memoriam of Mario Sorolla.

*Email address: miguel.beruete@unavarra.es
†Email address: pablo.rodriguez@unavarra.es
‡Email address: jazzsax.pacheco@hotmail.com
§Email address: m.navarro@imperial.ac.uk
‖Email address: aeserebr@googlemail.com

[1] R. E. Collin, *Field Theory of Guided Waves*, 2nd ed. (IEEE Press, New York, 1991).
[2] S. A. Schelkunoff and H. T. Friis, *Antennas. Theory and Practice* (Wiley, New York, 1966).
[3] E. Yablonovitch, Phis. Rev. Lett. **58**, 2059 (1987).
[4] J. D. Joannopoulos, P. R. Villeneuve, and S. Fan, Nature **86**, 143 (1997).
[5] J. B. Pendry, A. J. Holden, D. J. Robbins, and W. J. Stewart, IEEE Trans. Microwave Theory Tech. **47**, 2075 (1999).
[6] R. Marqués, F. Martín, and M. Sorolla, *Metamaterials with Negative Parameters: Theory, Design, and Microwave Applications* (John Wiley & Sons, New York, 2008).
[7] L. Solymar and E. Shamonina, *Waves in Metamaterials* (Oxford University Press, New York, 2009).
[8] T. W. Ebbesen, H. J. Lezec, H. Ghaemi, T. Thio, and P. A. Wolf, Nature **391**, 667 (1998).
[9] M. Beruete, M. Sorolla, I. Campillo, J. S. Dolado, L. Martín-Moreno, J. Bravo-Abad, and F. J. García-Vidal, Opt. Lett. **29**, 2500 (2004).

[10]M. Beruete, M. Sorolla, and I. Campillo, Opt. Express **14**, 5445 (2006).
[11]M. Beruete, I. Campillo, M. Navarro-Cía, F. Falcone, and M. Sorolla, IEEE Trans. Antennas Propag. **55**, 1514 (2007).
[12]R. Marqués, L. Jelinek, F. Mesa, and F. Medina, Opt. Express **17**, 11582 (2009).
[13]M. Beruete, M. Navarro-Cía, and M. Sorolla, Photonics Nanostruct. Fundam. Appl. **10**, 263 (2012).
[14]R. W. Wood, Philos. Mag. **4**, 396 (1902).
[15]F. J. García-Vidal, E. Moreno, J. A. Porto, and L. Martín-Moreno, Phys. Rev. Lett. **95**, 103901 (2005).
[16]J. C. Prangsma, D. V. Oosten, R. J. Moerland, and L. Kuipers, New J. Phys. **12**, 013005 (2010).
[17]J. Parsons, I. R. Hooper, W. L. Barnes, and J. R. Sambles, J. Mod. Opt. **56**, 1199 (2009).
[18]H. G. Booker, J. IEE (London), part IIIA, **93**, 620 (1946).
[19]C. A. M. Butler, J. Parsons, J. R. Sambles, A. P. Hibbins, and P. A. Hobson, Appl. Phys. Lett. **95**, 174101 (2009).
[20]C. S. R. Kaipa, A. B. Yakovlev, F. Medina, F. Mesa, C. A. M. Butler, and A. P. Hibbins, Opt. Express **18**, 13309 (2010).
[21]V. Torres, P. Rodríguez-Ulibarri, M. Navarro-Cía, and M. Beruete, Appl. Phys. Lett. **101**, 244101 (2012).
[22]L. V. Hau, S. E. Harris, Z. Dutton, and C. H. Behroozi, Nature **397**, 594 (1999).
[23]T. F. Krauss, Nature Photon. **2**, 448 (2008).
[24]K. L. Tsakmakidis, A. D. Boardman, and O. Hess, Nature **450**, 397 (2007).
[25]J. B. Khurgin, J. Opt. Soc. Am. B **22**, 1062 (2005).
[26]T. Baba, Nat. Photonics **2**, 465 (2008).
[27]A. Sakai, G. Hara, and T. Baba, Jpn. J. Appl. Phys. **40**, L383 (2001).
[28]A. Figotin and I. Vitebsky, Phys. Rev. E **63**, 066609 (2001).
[29]A. Figotin and I. Vitebsky, J. Magn. Magn. Mater. **300**, 117 (2006).
[30]M. Navarro-Cía, V. Torres, M. Beruete, and M. Sorolla, Prog. Electromagn Res. **118**, 287 (2011).
[31]www.cst.com.
[32]N. Engheta and R. W. Ziolkowski, *Metamaterials: Physics and Engineering Explorations* (Wiley, New York 2006).
[33]E. Prodan, C. Radloff, N. J. Halas, and P. Nordlander, Science **302**, 419 (2003).
[34]R. Ortuño, C. García-Meca, F. J. Rodríguez-Fortuño, J. Martí, and A. Martínez, Phys. Rev. B **79**, 075425 (2009).
[35]F. Medina, F. Mesa, and R. Marqués, IEEE Trans. Microwave Theory Tech. **56**, 3108 (2008).
[36]V. Lomakin and E. Michielssen, Phys. Rev. B **71**, 235117 (2005).
[37]M. Born and E. Wolf, *Principle of Optics*, 7th expanded ed. (Cambridge Univ. Press, Cambridge, 1999).
[38]H. Caglayan, I. Bulu, and E. Ozbay, Opt. Express **13**, 7645 (2005).